SF2A 2017
C. Reylé, P. Di Matteo, F. Herpin, É. Lagadec, A. Lançon, Z. Meliani, F. Royer (eds)

IMPACT OF CONVECTION AND RESISTIVITY ON ANGULAR MOMENTUM TRANSPORT IN DWARF NOVAE.

N. Scepi[1], G. Lesur[1], G. Dubus[1] and M.Flock[2]

Abstract. The eruptive cycles of dwarf novae are thought to be due to a thermal-viscous instability in the accretion disk surrounding the white dwarf. This model has long been known to imply enhanced angular momentum transport in the accretion disk during outburst. This is measured by the stress to pressure ratio α, with $\alpha \approx 0.1$ required in outburst compared to $\alpha \approx 0.01$ in quiescence. Such an enhancement in α has recently been observed in simulations of turbulent transport driven by the magneto-rotational instability (MRI) when convection is present, without requiring a net magnetic flux. We independently recover this result by carrying out PLUTO MHD simulations of vertically stratified, radiative, shearing boxes with the thermodynamics and opacities appropriate to dwarf novae. The results are robust against the choice of vertical boundary conditions. In the quiescent state, the disk is only very weakly ionized so, in the second part of our work, we studied the impact of resistive MHD on transport.We find that the MRI-driven transport is quenched ($\alpha \approx 0$) below the critical density at which the magnetic Reynolds number $R_{\rm m} \leq 10^4$. This is problematic because the X-ray emission observed in quiescent systems requires ongoing accretion onto the white dwarf.

Keywords: accretion disks, convection, turbulence , magnetohydrodynamics (MHD), dwarf novae

1 Introduction

A fundamental, yet challenging, issue in accretion theory is the transport of angular momentum. Historically, the transport of angular momentum has been parametrized by the dimensionless parameter α, the ratio of the fluid stress (responsible for the transport) to the local thermal pressure (Shakura & Sunyaev 1973).

Dwarf novae (DNe) provide the best observational constrains on α (King et al. 2007). DNe are binary systems where matter is transferred by Roche lobe overflow from a solar-type star to a white dwarf. Their lightcurves show periodic outbursts during which the luminosity typically rises by several magnitudes (Warner 2003). According to the disk instability model (DIM, see Lasota 2001 for a review), these outbursts are caused by a thermal-viscous instability in the accretion disk due to the steep temperature dependence of the opacity when hydrogen ionizes around 7000 K. Outburst decay timescales imply $\alpha \sim 0.1$ (Kotko & Lasota 2012) whereas recurrence timescales imply $\alpha \sim 0.01$ in quiescence (Cannizzo et al. 1988, 2012). Although it has long been known that the DIM requires transport to be more efficient in outburst than in quiescence (Smak 1984), the physical reason for this change in α has remained elusive.

It is now widely accepted that angular momentum transport in disks is due to turbulence driven by the development of the magneto-rotational instability (MRI, Balbus & Hawley 1991). Stratified local simulations (isothermal or with an artificial cooling) with zero net magnetic flux show a universal value of $\alpha \sim 0.03$ (Simon et al. 2012, Latter & Papaloizou 2012), comparable to the value required for quiescent DNe. To properly investigate the thermal equilibrium states of DNe, Hirose et al. (2014) performed the first simulations including radiative transfer, vertical stratification and the realistic thermodynamics appropriate to DNe. They found that convection increases α to 0.1 in the hot state's low density part, in the absence of net magnetic flux, providing a tantalizing solution to the change in α in DNe (Coleman et al. 2016).

Another explanation for the difference in transport efficiency between hot and cold states was proposed by Gammie & Menou (1998). In the quiescent state of DNe, the plasma is expected to be largely neutral and thus

[1] Univ. Grenoble Alpes, CNRS, Institut de Planétologie et d'Astrophysique de Grenoble (IPAG), F-38000, Grenoble, France
[2] Jet Propulsion Laboratory, California Institute of Technology, Pasadena, California 91109, USA

the magnetic field decouples from the disk. With the electron fraction a strong function of the temperature, they pointed out that the MRI may not be able to grow or, at least, sustain fully developed turbulence in a quiescent DNe disk.

In light of these results, we have carried out numerical simulations to assess the impact of convection and resistivity on the transport of angular momentum in DNe in the hot, outburst and cold, quiescent states (respectively).

2 Framework

2.1 Model

We adopt the local, shearing-box approximation (Hawley et al. 1995), to simulate a vertically-stratified patch of accretion disk situated at a distance $R_0 = 1.315 \times 10^{10}$ cm from a $0.6\,M_\odot$ white dwarf. In the co-rotating frame, the radiative MHD equations are :

$$\frac{\partial \rho}{\partial t} + \boldsymbol{\nabla} \cdot (\rho \boldsymbol{v}) = 0 \tag{2.1}$$

$$\rho \frac{\partial \boldsymbol{v}}{\partial t} + (\rho \boldsymbol{v} \cdot \boldsymbol{\nabla}) \boldsymbol{v} = -\boldsymbol{\nabla} \left(P + \frac{B^2}{8\pi} \right) + \left(\frac{\mathbf{B}}{4\pi} \cdot \boldsymbol{\nabla} \right) \mathbf{B} + \rho \big(-2\Omega \hat{\boldsymbol{z}} \times \boldsymbol{v} + 3\Omega^2 x \hat{\boldsymbol{x}} - \Omega^2 z \hat{\boldsymbol{z}} \big) \tag{2.2}$$

$$\frac{\partial E}{\partial t} + \boldsymbol{\nabla} \cdot [(E + P_t)\boldsymbol{v} - (\boldsymbol{v} \cdot \mathbf{B})\mathbf{B}] = -\rho \boldsymbol{v} \cdot \boldsymbol{\nabla} \Phi - \kappa_P \rho c (a_R T^4 - E_R) \tag{2.3}$$

$$\frac{\partial \mathbf{B}}{\partial t} = \boldsymbol{\nabla} \times (\boldsymbol{v} \times \mathbf{B} - \frac{4\pi}{c} \eta \mathbf{J}) \tag{2.4}$$

$$\frac{\partial E_R}{\partial t} - \boldsymbol{\nabla} \frac{c\lambda(R)}{\kappa_R \rho} \boldsymbol{\nabla} E_R = \kappa_P \rho c (a_R T^4 - E_R) \tag{2.5}$$

The last three terms of Eq. 2 represent, respectively, the Coriolis force, the tidal force and the vertical component of the gravitational force.

2.2 Method

We solve the MHD equations on a 3D Cartesian grid with the conservative, Godunov-type code PLUTO (Mignone 2009). Radiative transfer is treated separately from the MHD step using an implicit time-stepping following Flock et al. (2013). In this step, we solve the coupled matter-radiation equations in the flux-limited diffusion approximation. Opacities, internal energy, mean molecular weight are computed using pre-calculated tables. For the MHD step, we use the HLLD Riemann solver and switch for HLL in region of high pressure gradient to improve the robustness of our code.

We use shear-periodic conditions in the x-direction, periodic conditions in the y-direction, and either periodic or modified outflow conditions (as in Brandenburg et al. (1995)) for the z-direction to test their influence on the results (Hirose et al. 2014 used only outflow conditions). Our boxes have a resolution of $32\times128\times256$, a size of $1.5H\times6H\times12H$ on the hot branch (see §3) and of $0.75H\times3H\times6H$ for the cold and middle branch (see §3) in x, y and z direction respectively.

We explore the parameter space in Σ and $T_{\rm eff}$ to retrieve the stability curve of the disk at R_0 and follow the evolution of α. We start from an isothermal simulation and activate radiative transfer after ~ 50 orbits. For certain runs in the hot branch's low density part, we restart from previous simulations and change surface density allowing a smoother transition to capture the disk equilibrium.

For non ideal runs, resistivity is computed consistently with a pre-calculated table and we use a minimum floor to avoid dramatically small time steps.

3 Results

3.1 Ideal MHD simulations

The simulations trace an equilibrium thermal curve in the shape of an S (an S-curve) with a hot, stable branch and a cold, stable branch, providing independent confirmation of the results of Hirose et al. (2014). The S-curve from the simulations is comparable to that predicted by the vertical structure calculations using an α-prescription. These also predict a third stable branch at intermediate temperatures ($T_{\rm mid} \approx 10^4$ K).The middle

branch is not as extended as the other branches and may be seen as a prolongation of the cold branch to higher temperatures.

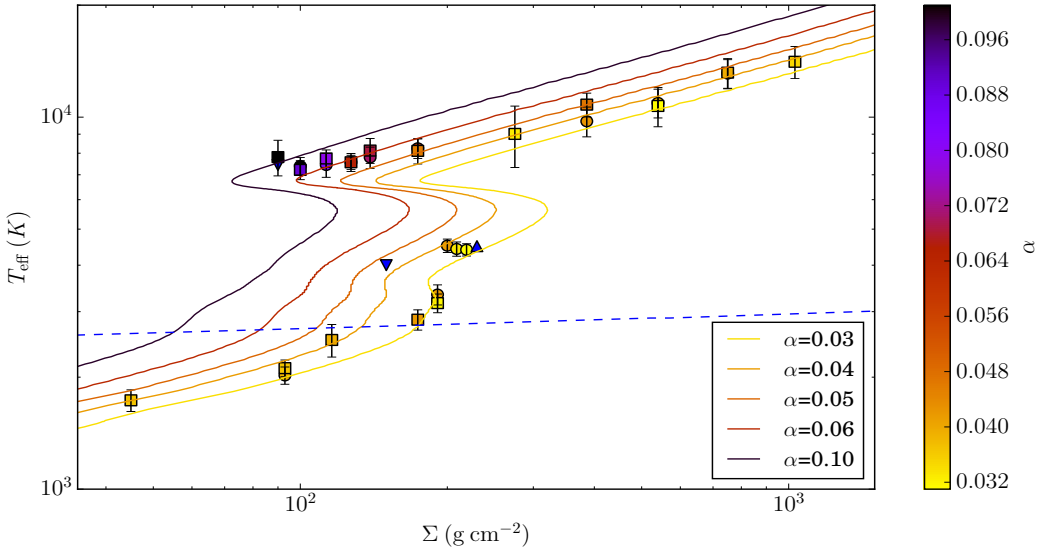

Fig. 1: Thermal equilibria in the $[T_{\rm mid}]$ vs $[\Sigma]$ (top) or $[T_{\rm eff}]$ vs $[\Sigma]$ (bottom) plane. Squares and circles are respectively for periodic and outflow runs. Triangular dots represent runs with runaway cooling (triangle facing down) or heating (triangle facing up). Error bars represent the standard deviation of the temperature fluctuations. The symbols are color-coded to the value of α. The color-coded curves are vertical thermal equilibria using an α-prescription. The dashed blue line indicates where the magnetic Reynolds number $R_m = 10^4$ based on an isothermal model.

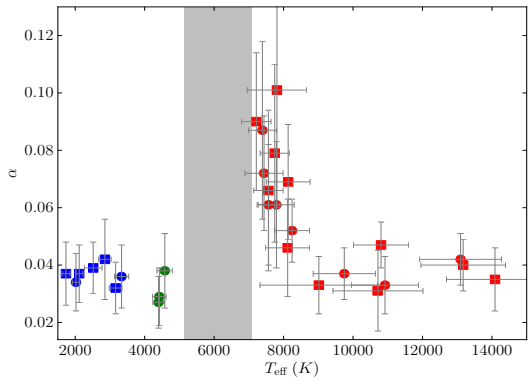

Fig. 2: α as a function of $[T_{\rm mid}]$ (top panel) and $[T_{\rm eff}]$ (bottom panel). Error bars represent the standard deviations of the fluctuations around the mean values. Blue, green and red colors are respectively for the cold, middle and hot branch. Squares and circles indicate periodic and outflow runs. The shaded area corresponds to the thermally-unstable region.

On Figure 1 and 2, we see an enhancement of α in the low Σ part of the hot branch, with a maximum value of $\alpha \approx 0.101$. Hirose et al. (2014) attributed the enhanced α to convection. We also observe that the enhanced α runs are convectively-unstable (Scepi et al. 2017) and further note that the value of α does not depend on the chosen vertical boundary conditions. Although convection plays a major role in transporting heat in the runs

with an enhanced α, we find no clear relationship between α and $f_{\rm conv}$, the average fraction of the flux carried by convection. Notably, α is not enhanced on the middle branch although it is strongly convectively-unstable (Scepi et al. 2017).

3.2 Resistive simulations

Ideal MHD may not apply to the cold branch due to the very low ionization fractions. The development of the MRI can be suppressed as the resistivity due to electron-neutral collisions increase. This is quantified by the magnetic Reynolds number

$$R_{\rm m} \equiv \frac{c_s h}{\eta} \tag{3.1}$$

with η the resistivity, c_s the sound speed and $h = c_s/\Omega$ the local pressure scale-height. For $R_{\rm m} < 10^4$, it is expected that diffusion of the magnetic field becomes too important for the disk to sustain MHD turbulence (Hawley et al. 1996; Fleming et al. 2000).

We find that resistivity has a critical impact by suppressing turbulence on the cold branch below some critical density located between $\Sigma = 174\,{\rm g\,cm^{-2}}$ and $\Sigma = 191\ {\rm g\,cm^{-2}}$. The dashed blue line on Figure 1 show the limit under which MRI should be stable from an isothermal model. There is very little discrepancy between our results and the model as in the cold branch the disk is almost isothermal.

4 Conclusion

In a first part, we find that the thermal equilibrium solutions found by the simulations trace the well-known S-curve derived from α-prescription models, including a middle branch that extends the cold branch to higher temperatures and is characterized by vigorous convection. We confirm that α increases to ≈ 0.1 near the unstable tip of the hot branch as reported by Hirose et al. (2014). This increase is thus robust against the choice of numerical code and, as we investigated, against the choice of outflow or periodic vertical boundary conditions. In the second part, we show that the region of the cold branch with $\Sigma < 191\,{\rm g\,cm^{-1}}$ does not maintain the MRI-driven turbulence. This is problematic because the X-ray emission observed in quiescent DNe requires ongoing accretion onto the white dwarf.

References

Balbus, S. A. & Hawley, J. F. 1991, The Astrophysical Journal, 376, 214
Brandenburg, A., Nordlund, A., Stein, R. F., & Torkelsson, U. 1995, ApJ, 446, 741
Cannizzo, J. K., Shafter, A. W., & Wheeler, J. C. 1988, The Astrophysical Journal, 333, 227
Cannizzo, J. K., Smale, A. P., Wood, M. A., Still, M. D., & Howell, S. B. 2012, The Astrophysical Journal, 747, 117
Coleman, M. S. B., Kotko, I., Blaes, O., Lasota, J.-P., & Hirose, S. 2016, MNRAS, 462, 3710
Fleming, T. P., Stone, J. M., & Hawley, J. F. 2000, The Astrophysical Journal, 530, 464
Flock, M., Fromang, S., González, M., & Commerçon, B. 2013, Astronomy & Astrophysics, 560, A43
Gammie, C. F. & Menou, K. 1998, The Astrophysical Journal Letters, 492, L75
Hawley, J. F., Gammie, C. F., & Balbus, S. A. 1995, ApJ, 440, 742
Hawley, J. F., Gammie, C. F., & Balbus, S. A. 1996, ApJ, 464, 690
Hirose, S., Blaes, O., Krolik, J. H., Coleman, M. S. B., & Sano, T. 2014, The Astrophysical Journal, 787, 1
King, A., Pringle, J., & Livio, M. 2007, Monthly Notices of the Royal Astronomical Society, 376, 1740
Kotko, I. & Lasota, J.-P. 2012, Astronomy & Astrophysics, 545, A115
Lasota, J.-P. 2001, New Astronomy Reviews, 45, 449
Latter, H. N. & Papaloizou, J. C. 2012, Monthly Notices of the Royal Astronomical Society, 426, 1107
Mignone, A. 2009, Memorie della Societa Astronomica Italiana Supplementi, 13, 67
Scepi, N., Lesur, G., Dubus, G., & Flock, M. 2017, ArXiv e-prints
Shakura, N. I. & Sunyaev, R. A. 1973, A&A, 24, 337
Simon, J. B., Beckwith, K., & Armitage, P. J. 2012, Monthly Notices of the Royal Astronomical Society, 422, 2685
Smak, J. 1984, Acta Astron., 34, 161
Warner, B. 2003, Cataclysmic variable stars, Vol. 28 (Cambridge University Press)